A&A 438, 187–199 (2005)
DOI: 10.1051/0004-6361:20042340

Astronomy & Astrophysics

Diffuse interstellar bands of unprecedented strength in the line of sight towards high-mass X-ray binary 4U 1907+09⋆,⋆⋆

N. L. J. Cox[1], L. Kaper[1], B. H. Foing[2], and P. Ehrenfreund[3,1]

[1] Astronomical Institute "Anton Pannekoek", University of Amsterdam, Kruislaan 403, 1098 SJ Amsterdam, The Netherlands
e-mail: ncox@science.uva.nl
[2] ESA/SCI-SR, ESTEC, PO Box 299, 2200 AG Noordwijk, The Netherlands
[3] Astronomy Institute, Radboud University Nijmegen, PO Box 9010, 6500 GL Nijmegen, The Netherlands

Received 9 November 2004 / Accepted 4 April 2005

Abstract. High-resolution VLT/UVES spectra of the strongly reddened O supergiant companion to the X-ray pulsar 4U 1907+09 provide a unique opportunity to study the nature of the diffuse interstellar bands (DIBs) at unprecedented strength. We detect about 180 known DIBs, of which about 25 were listed as tentative and are now confirmed. A dozen new DIB candidates longwards of 6900 Å are identified. We show that the observed 5797 Å DIB strength is in line with the Galactic correlation with reddening, whereas the 5780 Å DIB strength is relatively weak. This indicates the contribution of denser regions, where the UV penetration is reduced. The presence of dense cloud cores is supported by the detection of C_2 rotational transitions. Members of one DIB family (5797, 6379 Å and 6196, 6613 Å) behave coherently, although one can make a distinction between the two correlated pairs. The broadened profiles of narrow DIBs are shown to be consistent with the premise that each of the main clouds in the line of sight discerned in the interstellar K I profile is contributing proportionally to the DIB profile. We complement and extend the relation of DIB strength with reddening $E_{(B-V)}$, as well as with neutral hydrogen column density N(H I), respectively, using strongly reddened sightlines towards another four distant HMXBs. The 5780 Å DIB, and tentatively also the 5797 and 6613 Å DIBs, are better correlated to the gas tracer H I than to the dust tracer $E_{(B-V)}$. The resulting relationship can be applied to any line of sight to obtain an estimate of the H I column density. In the search for the nature of the DIB carrier, this strongly reddened line of sight is a complementary addition to single cloud line of sight studies.

Key words. ISM: lines and bands – X-rays: individual: 4U 1907+09

1. Introduction

Superimposed on the visual to near infrared (4000–10 000 Å) interstellar extinction curve are numerous broad to narrow unidentified absorption bands (about 200 confirmed and 70 tentative detections, e.g. Jenniskens & Desert 1994; Tuairisg et al. 2000; Galazutdinov et al. 2000). These diffuse interstellar bands (DIBs) remain one of the oldest mysteries in stellar spectroscopy. Not one DIB carrier has of yet been unambiguously identified, although many candidates exist (see review by Herbig 1995). Heavily obscured lines of sight can provide valuable information on the environmental conditions and nature of the DIB carriers, as the light probes a large column of gas and dust piercing far into the Milky Way. Our interest in 4U 1907+09 was prompted by previous studies (e.g. Van Kerkwijk et al. 1989) that, although reporting spectra with modest resolving power and signal-to-noise, revealed several extremely strong DIBs. The optical counterpart to the X-ray pulsar 4U 1907+09 (Giacconi et al. 1971) is a heavily reddened massive star (V = 16.4 mag) showing broad Hα emission (Schwartz et al. 1980), identifying the system as a high-mass X-ray binary (HMXB). A detailed investigation of the binary system parameters, including the determination of the O8/9 Ia spectral type of the primary is presented in a companion paper (Cox et al. 2005). With a distance of about 5 kpc and reddening $E_{(B-V)} = 3.45$ mag, or visual extinction A_V = 9.5 mag (Cox et al. 2005), 4U 1907+09 provides a unique opportunity to probe a large column of interstellar gas and dust. The optical spectrum of 4U 1907+09 includes a very rich variety of interstellar absorption lines, and contains only few stellar lines, making it an excellent target to study the interstellar medium (ISM) in general, and DIBs in particular.

In this paper we present high-resolution optical spectra of the interstellar line of sight towards the massive companion to 4U 1907+09 obtained with the Ultraviolet and Visual Echelle Spectrograph (UVES[1]; Kaufer et al. 2000) mounted at the *Very Large Telescope* (VLT) of the European Southern Observatory

⋆ Based on VLT/UVES observations collected at the European Southern Observatory, Paranal, Chile (ESO programs 60.A-9022, 63.H-0456 and 67.C-0281).

⋆⋆ Full Table 2 is only available in electronic form at http://www.edpsciences.org

[1] www.eso.org/instruments/UVES/

in Paranal, Chile. The observations and the data reduction procedures are described in the next section (Sect. 2). Section 3 presents the observed interstellar DIB spectrum. In Sect. 4 a detailed analysis of the diffuse interstellar bands (DIBs) observed towards 4U 1907+09 is given. The observations show DIBs of unprecedented strength, and also allow us to confirm the presence of many weak DIBs (Sect. 4.1). Section 4.2 discusses the DIB strength versus reddening $E_{(B-V)}$ (a common indicator for the amount of dust in a line of sight). In addition, we investigate the behaviour of DIBs that are known to show correlated behaviour (Sect. 4.3). The 5780 and 5797 Å DIB strengths or central depths can be used to infer the properties of the effective local UV field and to differentiate between diffuse and denser cloud regions (Sect. 4.4). In Sect. 4.5 we discuss the Doppler broadening of DIBs as a result of the velocity gradient of the interstellar medium in this extended line of sight. We show, for example, that neutral potassium is a good tracer of the 6613 and 5797 Å DIB carriers. In the last part, Sect. 4.6, we elaborate on the relationship between DIB strengths and the K I and H I column densities. The discussion then argues how heavily reddened lines of sight, and the one towards 4U 1907+09 in particular, provide new insight into the physicochemical properties of the DIB carrier.

2. Observations and data reduction

High-resolution ($R \sim 40\,000$) spectra of the optical companion to the X-ray pulsar 4U 1907+09 were obtained with UVES during the nights of 24 to 27 September, 2001 (ESO program 67.C-0281). Observations were performed under excellent conditions at Paranal, with a relative humidity of less than 10% and seeing between 0.4 and 0.8 arcsec. The total exposure time on 4U 1907+09 was 9000 s (for observational details see Table 1). Two spectra of bright B stars were taken before the exposures of 4U 1907+09. These spectra are used for the correction for telluric absorption lines, as described below. Relevant properties of the optical companion to 4U 1907+09 and the two standard targets are listed in Table 1.

The spectra were reduced using the UVES context within the MIDAS reduction package (version 02SEPpl1.2), which allowed us to apply the UVES data reduction pipeline[2] software and to adapt and fine tune, if necessary, the standard procedures. The resulting signal-to-noise ratio (S/N) ranges from ~30 in the green continuum to about 150 in the red continuum, and down again in the NIR. The wavelength calibration is done by identifying ThAr arc lines in calibration exposures taken for each CCD and set-up. The root mean square of the fitted lines is approximately 0.003 Å and 0.008 Å in the blue and red arm, respectively. We found no significant quality differences between the manual step-by-step reduction and the products delivered by the pipeline. For most orders the merging process performs well, even for broader features spanning over two orders. However, one should be cautious with any features in regions where the echelle orders overlap (i.e. the order edges) because this can give rise to artifacts. For the features of interest in this study, in most cases the orders need not be merged at all.

[2] www.eso.org/observing/dfo/quality/

Table 1. Properties of the observed target 4U 1907+09 and the telluric standards HD 165470 and HD 166934. The listed values were obtained from the SIMBAD database, except $E_{(B-V)}$, $v_r \sin i$ and spectral type of the optical companion to 4U 1907+09 which were taken from Cox et al. (2005). The intrinsic colours for the quoted spectral types are adopted from Schmidt-Kaler (1982). The total exposure time for 4U 1907+09 is 9000 s; 6300 and 2700 s in the 346+580 and 437+860 settings, respectively. The instrument settings are indicated by the central wavelength (in Å) of the red and blue arm of the UVES spectrograph, respectively. The former setting covers the spectral range up to 6640 Å, while the latter covers the spectral range, with gaps, from 6700 to 10390 Å (shown in Fig. 1).

	4U 1907+09	HD 165470	HD 166934
l (deg)	43.74	353.92	11.96
b (deg)	0.48	–8.79	–0.51
V (mag)	16.4	7.34	8.8
$B-V$ (mag)	3.17	–0.17	–0.2
Spectral type	O8-O9 I	B2 III	B2 IV/V
$(B-V)_0$ (mag)	–0.28	–0.24	–0.24
$E_{(B-V)}$ (mag)	3.45	0.07	0.04
A_V (mag)	9.3	0.22	0.12
$v_r \sin i$ (km s^{-1})	100 ± 5	43 ± 3	54 ± 4
Total exposure time (s)	9000	200	760
UT at start			
(2001-09-day/h:m:s)	24/01:02:02	23/23:30:40	23/23:47:54
	26/01:48:35		
	27/00:57:36		
	27/01:28:32		
Airmass	1.3–1.8	1.055	1.055

Several regions in the spectrum are heavily contaminated with atmospheric telluric lines. For example, there is an O_2 bandhead around 6280 Å, although most telluric lines are present between 7600 and 9800 Å. Contaminated regions were corrected for telluric lines via division by an unreddened standard star. Note that the photospheric spectrum of the telluric standard star (of spectral type B) would be divided out as well; therefore, before applying the correction we remove the photospheric lines from the standard spectrum by applying a standard "continuum" spline. We use two standards to check for possible artifacts resulting from the division. The original spectrum is divided by the telluric standard raised to the power α, where we take the ratio of the airmass of both observations as the initial guess. To improve the spectrum further it was necessary to shift the telluric standard spectrum by a small amount, typically a fraction of a wavelength bin. The optimum values for both the airmass correction factor α and the wavelength shift were obtained, for each order separately, using an iterative procedure that minimises the residual telluric line features.

3. Observed DIB spectrum and its synthetic counterpart

This section describes the quality and properties of the obtained spectra. Unfortunately, due to the heavy reddening the blue spectra are of poor quality. Therefore, the spectrum effectively

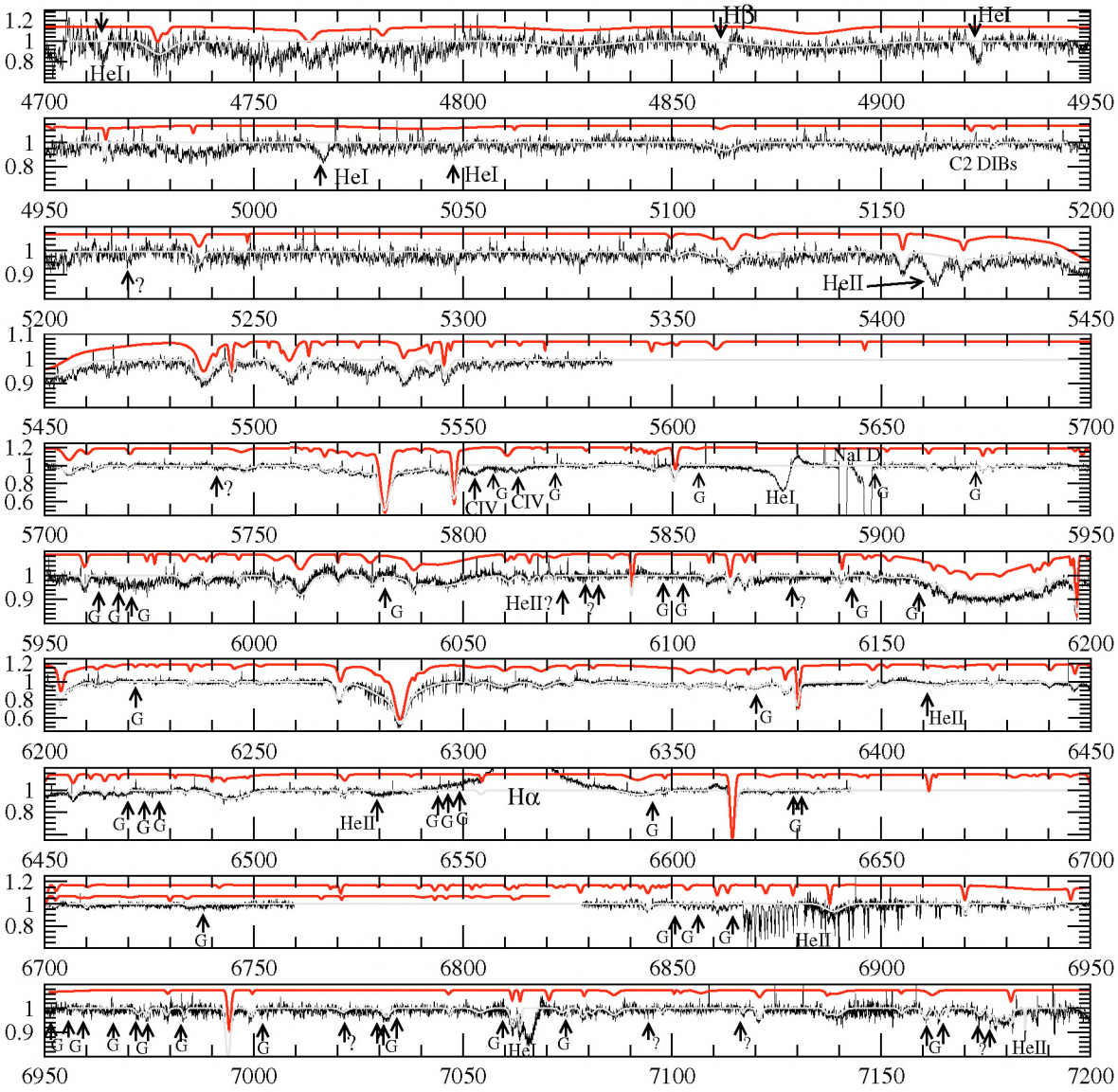

Fig. 1. The normalised spectrum of 4U 1907+09 from 4700 Å to 7200 Å. Arrows labelled **"?"** indicate unidentified features; those labelled **"G"** refer to the position of candidate DIBs, from the Galazutdinov et al. (2000) survey, that are not listed by Tuairisg et al. (2000) for BD +63 1964. The synthetic DIB spectrum of BD +63 1964 ($E_{(B-V)}$ = 1.01 mag; Tuairisg et al. 2000) is scaled to the reddening of 4U 1907+09 and shown with a small offset (continuum is unity), shortwards of 6820 Å. Longwards of 6700 Å the DIB spectrum of HD 183143 is shown ($E_{(B-V)}$ = 1.28 mag; Jenniskens & Desert 1994), scaled to the reddening of 4U 1907+09. Both synthetic spectra are also redshifted to match the observed DIB positions. Note the detail and wealth of the DIBs in all spectra. Figure 3 gives a close-up of four strong DIBs. Stellar photospheric and wind lines are identified by the corresponding atom/ion (see also Cox et al. 2005). Gaps in the spectral coverage are due to gaps between orders, between the three CCD detectors, and between UVES settings. The synthetic constructed DIB spectrum for 4U 1907+09, derived from Table 2 and shown in its entirety in Fig. 2, is plotted in light grey on top of the observed spectrum.

starts in the green ($\lambda \sim 4700$ Å). Figure 1 shows the entire spectrum of 4U 1907+09 from 4700 Å to 10 400 Å. This spectrum is an average of all available spectra, corrected for telluric lines where appropriate, and smoothed with a 5 or 7-pixel (0.10 or 0.15 Å) running mean at wavelengths shortwards of 6800 Å. All identified stellar (e.g. H I, He I, He II, C III and C IV) and interstellar (Na I, K I) atomic lines are labelled accordingly. For a discussion of the photospheric spectrum we refer to Cox et al. (2005) . We inspected a model atmosphere spectrum (with T = 30 000 K, $\log g$ = 3.00 and $v_r \sin i$ = 100 km s^{-1}) computed by Lanz & Hubeny (2003) for possible stellar contamination of the DIB spectrum, up to 7500 Å. Although this model atmosphere does not reproduce the H I and He I lines as good as the stellar atmosphere model applied in Cox et al. (2005), it is useful to identify weak stellar lines originating from heavy elements not included in the latter. We identify only 9 possible weak stellar features (including 4 He II lines) that (1) coincide with observed DIBs; (2) are stronger than 10 mÅ; and (3) have central depths larger than 1% (see Table 2).

For the DIB identification we use the synthetic DIB spectrum of BD +63 1964 ($E_{(B-V)}$ = 1.01 mag; Tuairisg et al. 2000) shortwards of 6800 Å, and that of the often used DIB

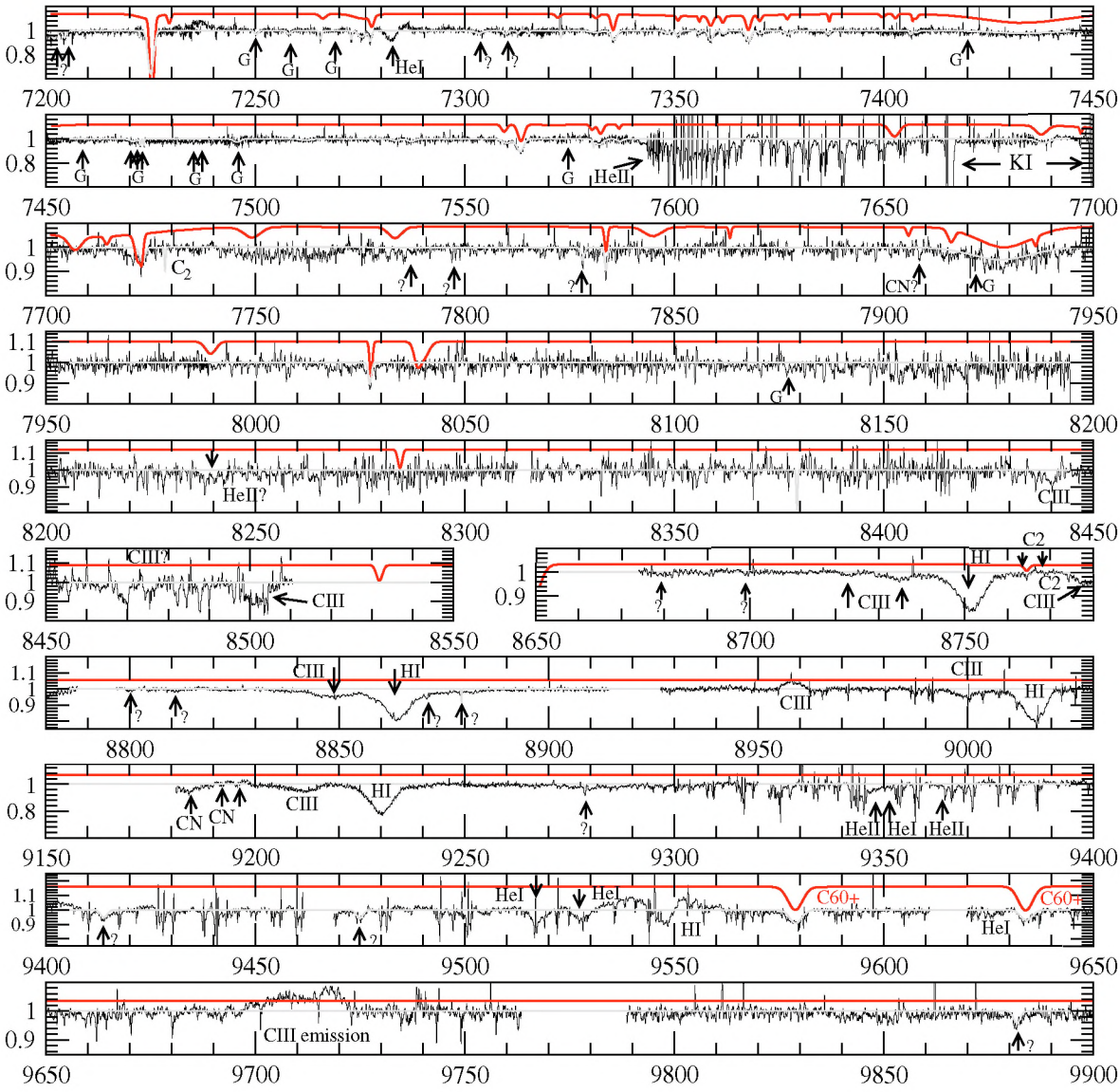

Fig. 1. continued. The normalised spectrum of 4U 1907+09 from 7200 Å to 9900 Å. Note that we observe the two DIBs at 9577 Å and 9632 Å that are tentatively attributed to the C_{60}^{+} molecule (Foing & Ehrenfreund 1994, 1997).

target HD 183143 ($E_{(B-V)} = 1.28$ smag; Jenniskens & Desert 1994 updated with Jenkins 1996 and Krełowski et al. 1995[3]) longwards of 6700 Å. The synthetic comparison spectra are computed from the listed central wavelength λ, equivalent width (*EW*) and full width at half maximum (*FWHM*). Both comparison spectra are scaled to the reddening of 4U 1907+09, redshifted to match observed DIB wavelengths, displaced vertically for clarity, and plotted in Fig. 1. We chose BD +63 1964 because it shows an overall enhancement of DIB strength displaying many tentative weak features which await confirmation. Also, both lines of sight are well studied and their characteristics are extensively documented in literature.

In order to identify any new features as DIBs, spectra of (high) reddening lines of sight are very helpful, because DIBs are enhanced in such environments, thus requiring spectra with less *S/N*. Alternatively, one could use spectroscopic binaries to identify stationary, and thus interstellar, lines. Since any new features will be either very weak or situated in telluric or stellar line regions, this imposes strict quality requirements on new spectroscopic observation strategies. The detection limit of features in these spectra varies widely over the entire wavelength range. The "red" part (5700–6700 Å) shows much detail, with features as weak as 5 mÅ, which can nevertheless only be positively identified using detailed comparison DIB spectra. In contrast, for many regions longwards of 7000 Å DIB detections are noise limited to features with strengths of tens to hundreds of mÅ, often due to "noise" introduced by the telluric line correction method.

Nevertheless, most of the DIBs (about 180) previously listed in the covered wavelength regions between 4700 and 9900 Å (Tuairisg et al. 2000; Jenniskens & Desert 1994) are

[3] See `http://leonid.arc.nasa.gov/DIBcatalog.html` for the updated DIB catalogue compiled by P. Jenniskens.

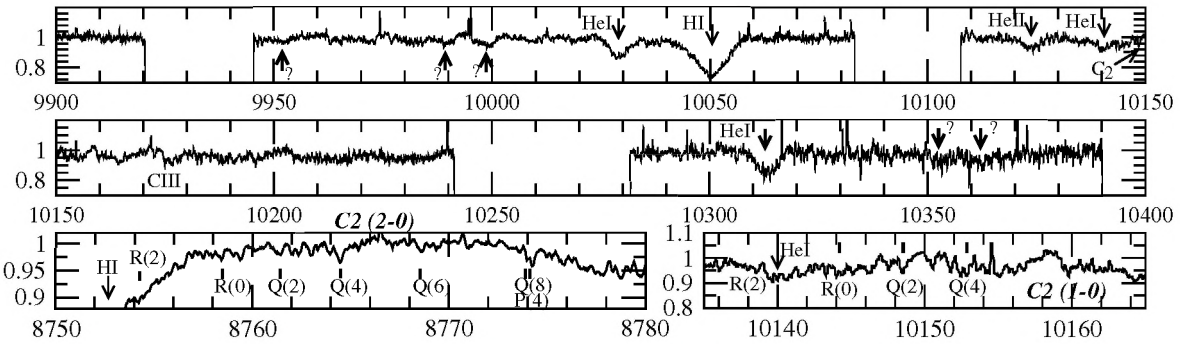

Fig. 1. continued. The normalised spectrum of 4U 1907+09 from 9900 Å to 10 400 Å. Weak narrow C_2 lines are seen near 8765 and 10148 Å. The bottom left and right panels show a zoomed view of the spectral ranges of these C_2 (2–0) and (1–0) Philips system transitions, respectively. See e.g. Van Dishoeck & Black (1989) and references therein for transition levels and wavelengths.

Table 2. Central wavelength λ (Å), full width at half maxium F (Å), equivalent width W (mÅ) and the error on the equivalent width σW (mÅ) for a selection of the strongest DIBs observed towards 4U 1907+09 and the comparison targets BD +63 1964 and HD 183143 (Tuairisg et al. 2000). The full table is available as on-line material only.

4U 1907+09 $E_{(B-V)}$ = 3.45 mag				BD +63 1964 $E_{(B-V)}$ = 1.01 mag				HD 183143 $E_{(B-V)}$ = 1.28 mag	
λ	F	W	σW	λ	F	W	σW	W	σW
5777.1	2.2	140	10	5776.21	2.00	28	4	19	4
5781.2	2.6	1170	30	5780.55	2.22	699	4	770	8
5795.7	0.9	50	4	5796.07	6.65	155	16	138	18
5797.8	1.4	539	8	5797.08	0.96	258	15	187	10
5850.3	1.4	250	29	5849.81	1.07	119	2	62	4
6196.8	1.3	206	3	6195.99	0.68	79	3	86	5
6203.8	1.6	275	6	6203.06	1.30	139	13	125	18
6205.1	5.9	589	6	6204.22	4.92	135	9	123	9
				6207.52	9.34	132	17	160	17
6270.5	2.6	538	7	6269.82	1.22	84	5	115	10
				6270.45	4.34	86	11	130	11
6283.9	11.73	2650	100	6283.30	10.1	899	45	1240	102
6285.1	3.0	830	20	6284.09	2.71	540	11	689	19
6302.9	1.94	81	20	6302.29	3.19	31	3	20	3
6377.1	1.9	217	5	6376.02	0.64	27	4	44	4
				6376.57	1.80	52	7	20	4
6379.8	1.1	291	5	6379.22	0.81	176	3	107	3
6614.5	1.6	730	12	6613.63	1.14	314	4	320	4

detected towards 4U 1907+09. This includes over 25 tentative DIBs, which can now be confirmed. The recent DIB survey by Galazutdinov et al. (2000) reports the central positions of an additional 58 new weak and narrow DIBs, that are not listed by Tuairisg et al. (2000) for BD+63 1964, and are also covered by our observations; fifteen of these are confirmed. Additionally, several features that remain unidentified are detected; these features are indicated with arrows labelled **"?"** in Fig. 1. Most of the known very broad (*FWHM* $\geq$ 8 Å) DIBs are also detected, with the notable exception of the famous "blue" 4430 Å DIB, which is beyond our wavelength coverage. The error on the *EW* of these broad features is relatively large due to the dependence on the choice of the continuum placement. We also detect the 9577 and 9632 Å DIBs (Fig. 1) which have previously been assigned to the C_{60}^+ molecule (Foing & Ehrenfreund 1994, 1997).

The central wavelength $\lambda_{\rm central}$ (Å), *FWHM* (Å) and equivalent width *EW* (mÅ) of the measured DIBs are listed in Table 2 (only a small excerpt is included here, the complete table is included in the on-line material), together with corresponding values from one of the two comparison spectra. *FWHM* were obtained by fitting a set of Gaussians to small spectral regions containing up to 9 features. For isolated DIBs the *EW*s are measured by straight line integration of the profile. *EW*s for blended DIBs are given by the individual Gaussian fit components. The total *EW* of the Gaussian components was compared, and if

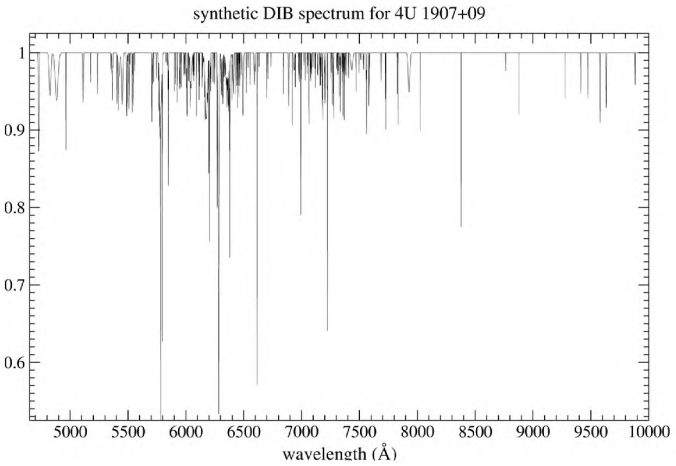

Fig. 2. Entire synthetic DIB spectrum (4650 to 9950 Å) for 4U 1907+09 generated from the 180 identified DIBs and measured absorption features and their respective central wavelength positions ($\lambda_{\rm DIB}$), equivalent widths (*EW*) and full width at half maximum (*FWHM*). This spectrum does not include stellar features nor atomic interstellar lines.

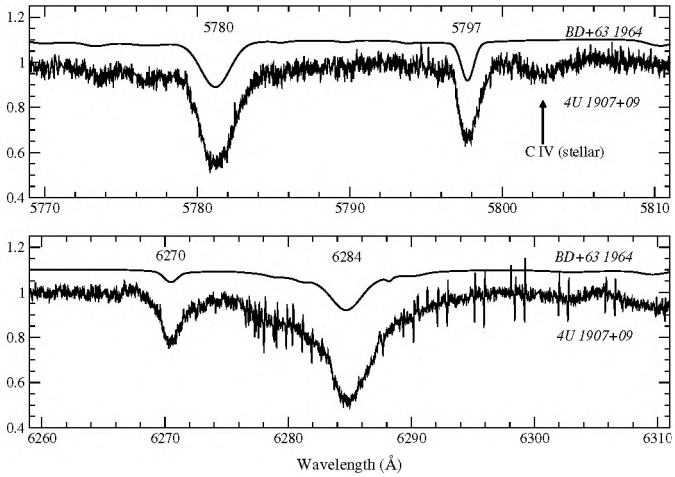

Fig. 3. Normalised spectra of four prominent DIBs (at 5780, 5797, 6270, 6284 Å) are shown. These illustrate the strength of DIBs in 4U 1907+09, as well as the spectral quality obtained. For comparison the synthetic spectrum of BD +63 1964 (Tuairisg et al. 2000) is plotted on top with a small vertical offset, and with a wavelength shift to match the 4U 1907+09 DIBs. The 6284 Å DIB has been corrected with the telluric standard star HD 165470. The small spikes on the spectrum (near and on the 6284 Å DIB) are the remnants of the telluric lines. See Sect. 2 for details on the telluric line correction method. The stellar C IV line at 5802 Å is characteristic of an O8/9 supergiant type (Cox et al. 2005).

necessary scaled, to the total *EW* derived by straight line integration of the entire blend, thus ensuring consistency with the results for the isolated DIBs. Strong, narrow or unblended DIBs (*EW* > 100 mÅ and *FWHM* < 2.0 Å) can be measured very accurately, and the errors are given by the statistical noise on the adjacent continuum. For the weaker and/or broader DIBs, and for DIB blends, the systematic errors due to inaccuracies in the continuum placement, normalisation and/or the Gaussian fitting procedure can be as much as 20% (see e.g. Galazutdinov et al. 2004). This makes it also difficult, or even impossible, to do a one-to-one DIB comparison for all DIBs between different lines of sight, as the systematic error is larger than the statistical error. The measured λ, *EW* and *FWHM* of the observed DIBs towards 4U 1907+09 result in a synthetically generated DIB spectrum for 4U 1907+09 (Fig. 2) that closely represents the observed DIB spectrum (Fig. 1).

4. Diffuse interstellar bands: Environmental behaviour

The identification of the DIB carrier(s) is the key goal of DIB research. In order to infer DIB carrier characteristics one can explore, as is done in this paper, the properties and behaviour of DIBs through complex and long lines of sight that probe large columns of interstellar material towards the center and the outer edges of the Galaxy. The behaviour of DIBs in the heavily reddened line of sight towards 4U 1907+09 is related to the general scheme/trend observed in the Galaxy in Sect. 5.

We discuss first the strength of the DIBs observed towards 4U 1907+09, and subsequently investigate the unique properties of this line of sight to study the link between DIBs and the local conditions of the ISM. The gas and dust in the Galactic spiral arms (e.g. Russeil 2003), which is associated with the multiple individual clouds (see K I profile in panel a of Fig. 5) in the direction of 4U 1907+09, contributes to the total DIB column, thus giving rise to their extraordinary strength. This overall increase in strength results in the detection of many weak DIBs, of which some were hitherto only tentative and are now confirmed DIBs (Sect. 3). Only with the advance of sensitive instruments and large telescopes, like UVES on the VLT, it has become possible to observe heavily reddened, distant, and therefore faint objects like 4U 1907+09.

4.1. Strongest DIBs observed

Until now, the strongest 5797, 5870, 6196, 6269 Å DIBs are observed towards Cyg OB2-27 (VI Cyg 10) and Cyg OB2-41 (VI Cyg 12) (Chlewicki et al. 1986), and the strongest 6203/4, 6284 and 6613 Å DIBs are detected towards the heavily reddened Stephenson targets StRS 177, StRS 354 and StRS 392 (Rawlings et al. 2003). For Cyg OB2-27 and Cyg OB2-41 only the 6269 and 6284 Å DIB are of comparable strength as those in 4U 1907+09. The 6284 Å DIB is stronger towards StRS 177 and StRS 354, although the reported large equivalent width errors for the latter two sightlines could be even larger due to difficulties in correcting for the telluric O_2 bandhead. There are also a few 4U 1907+09 DIBs (e.g. at 9577 and 9632 Å) that are of similar strength as those observed towards some less reddened Galactic targets, like HD 183143. Nevertheless, overall the DIBs observed towards 4U 1907+09 are the strongest measured to date. It is now for the first time that the complete and detailed DIB spectrum (including a broad range of features: from weak to strong, from narrow to broad) in such a highly reddened line of sight has been observed.

A selection of four DIBs is shown in more detail in Fig. 3, in order to illustrate their strength (equivalent width and central depth), as well as the spectral quality (*S/N* and resolution)

achieved. The 5780 and 6284 Å bands are two strong, intermediately broad and featureless DIBs (2 Å < $FWHM_{\text{single cloud}}$ < 7 Å), while the 5797 Å band is typical of a narrow ($FWHM_{\text{single cloud}}$ < 2 Å) strong DIB (others are for example the 6613 and 6379 Å DIBs). These DIBs are the most important, and best studied bands in understanding the DIB carrier's local environment (see Sect. 4.3) and its physical properties. Note that the central depth of the 5797, 5780 and 6284 Å DIBs are 0.34, 0.45 and 0.49, compared to 0.18, 0.21 and 0.19 for BD +63 1964, i.e. twice as deep.

4.2. DIB strength versus reddening

One of the most straightforward comparisons is DIB strength versus reddening $E_{(B-V)}$. For highly reddened lines of sight the strength of some DIBs increases roughly linearly with reddening, whereas others do not. The current idea is that the latter DIBs reside in relatively more dense clouds or diffuse cloud cores than the former, an effect that becomes more pronounced when the reddening increases (Herbig 1993). For example, certain carriers are more sensitive to the strength of the penetrating UV field than others; this behaviour will be discussed further in Sect. 4.4. The relation between DIB strength and reddening is not well determined at high values of $E_{(B-V)}$, because data points are scarce and measurement errors often large (e.g. Herbig 1995, and Fig. 4). Also, these studies have only been applied to a small number of DIBs, most notably the 5797 and 5780 Å DIBs and, although to a much lesser extent, the 6284 and 6613 Å DIBs.

For 4U 1907+09 the equivalent widths per unit reddening are on average closer to those measured in HD 183143 than those in BD +63 1964. The latter line of sight has specific local ISM conditions that favour the DIB carrier formation (Ehrenfreund et al. 1997). Figure 4 shows the Galactic trend of the 5780, 5797 and 6613 Å DIBs with respect to the reddening. Both the 5797 and 6613 Å DIBs, towards 4U 1907+09, have strengths expected from the extrapolation of the respective Galactic trends. This is consistent with previous studies that found an intermediate correlation between 5797 Å DIB strength and reddening $E_{(B-V)}$. Nevertheless, one can see a clear trend of increased DIB strength for larger amounts of dust and gas in the line of sight, as measured by the reddening. The 5780 Å DIB is significantly weakened with respect to the linear trend. This weakening of the 5780 Å DIB with respect to the 5797 Å DIB can be used to infer information on the local ionisation balance (Sect. 4.4).

4.3. Families or groups of DIBs: Signs of coherent behaviour?

Instead of comparing the strength of one or two DIBs in many lines of sight, it is interesting to compare a larger set of (strong) DIBs observed in the two lines of sight towards 4U 1907+09 and BD +63 1964 (or HD 183143), respectively. In this way DIBs can be grouped into so called families according to their mutual response, i.e. whether they behave similarly to different environmental ISM conditions. Coherent behaviour would indicate that the respective DIB carriers may have closely related physical or chemical properties, like ionisation potential, structural stability, geometry, size, etc.

There are indications of three main groups or families among the DIBs: (1) the 5797, 5849, 6196, 6379 and 6613 Å DIB family; (2) the 5780, 6284 and 6203 Å DIB family; and (3) the 4501, 5789, 6353 and 6792 Å DIB family (e.g. Josafatsson & Snow 1987; Krełowski & Walker 1987; Cami et al. 1997; Porceddu et al. 1991; Moutou et al. 1999; Wszołek & Godłowski 2003). Members of the first family have narrow profiles with a sub-structure that is indicative of a gas-phase molecule (Sarre et al. 1995; Ehrenfreund & Foing 1996), while members of the second family have no apparent substructure (e.g. Cami et al. 1997). The third family consists of weak DIBs for which the presence of substructure in the line profiles is not yet certain. DIBs of these families correlate reasonably well with their own family members, but not with those from the other families. Moutou et al. (1999) find a strong correlation in strength of the 6613 and 6196 Å DIB, and only marginal correlations for other pairs, consistent with results of Cami et al. (1997). In addition, the 5780 and 6284 Å DIBs represent the strongest DIBs that show no apparent substructure, and, although not strongly correlated, often show similar behaviour. This lack of a strong correlation suggests that each strong DIB results from an individual carrier molecule, which may still have similar physical/chemical properties, thus responding coherently to differences in environmental conditions.

For ten strong DIBs Table 3 lists the strength ratio between 4U 1907+09 and the two comparison targets. Evidently, this ratio varies among the DIBs. The overall DIB strength for 4U 1907+09 is a factor 2.25 and 1.95 higher, compared to the DIB strengths for HD 183143 and BD +63 1964, respectively. Compared to BD +63 1964 the 4U 1907+09 DIBs do not appear to behave coherently within families. The HD 183143 and 4U 1907+09 DIBs, on the other hand, do show consistent coherent behaviour among (sub)families. For example, within the first family there are two distinct pairs of strongly correlated DIBs (5797 and 6379 Å and 6196 and 6613 Å), and most family (1) members are enhanced by factor close to that of the increase in reddening. The strength of family (2) DIBs is much less enhanced than that of family (1) DIBs (see also Fig. 4). The 5780 and 6284 Å DIBs (family 2) are weakly correlated, and both show a similar DIB strength enhancement. If and how the weak DIBs (family 3) correlate with eachother, strong DIBs and environmental parameters can not yet be resolved due to a lack of data of sufficient quality and quantity. In conclusion, the strong DIBs towards 4U 1907+09, listed in Tables 2 and 3, have, compared to the reference targets, a smaller strength per unit reddening. Furthermore, the designation of DIBs to one of three families is too simplified; there is clear evidence that within families there are pairs of DIBs that behave less or more coherently, while other pairs do not.

The strong narrow 5797 and 6379 Å DIBs show the least weakening with respect to reddening, which implies that denser cloud parts exist in the line of sight where these DIB carriers are subsequently protected from the UV radiation. On the other hand, the presence of strong 5780 and 6284 Å DIBs requires strong UV radiation (Sect. 4.4). Thus the interstellar medium

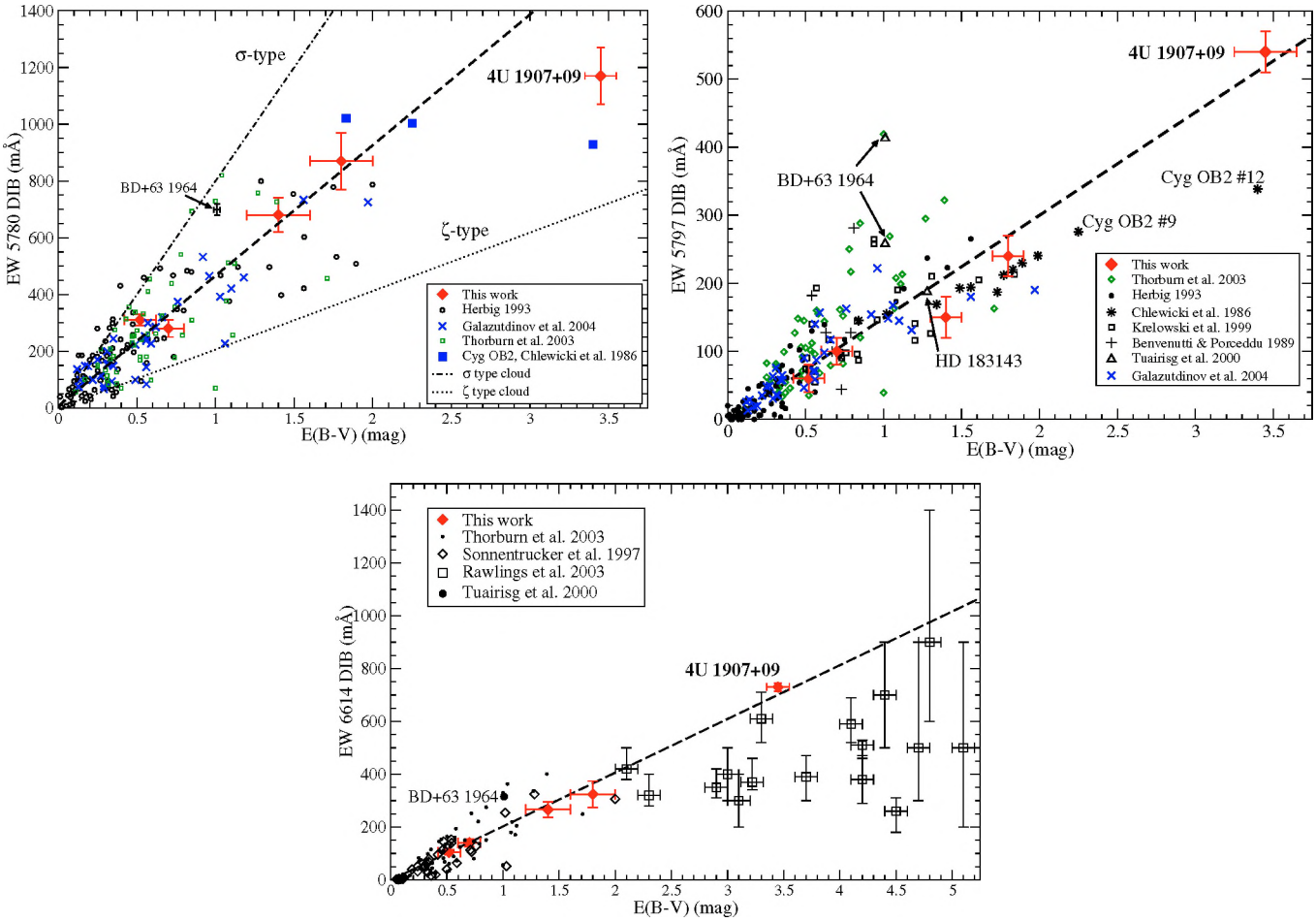

Fig. 4. Equivalent width of the 5780 Å (*top left panel*), 5797 Å (*top right panel*) and 6613 Å (*bottom panel*) DIBs as a function of reddening $E_{(B-V)}$ for Galactic sightlines. The 5780 Å DIB strengths are taken from Herbig 1993 (○), Chlewicki et al. 1986 (■), Thorburn et al. 2003 (□), Galazutdinov et al. 2004 (×) and this work (◆, see Table 4). The 5797 Å DIB data points are taken from Chlewicki et al. 1986 (∗), Herbig 1993 (○), Krełowski et al. 1999 (□), Benvenuti & Porceddu 1989 (+), Thorburn et al. 2003 (◇), Tuairisg et al. 2000 (△), Galazutdinov et al. 2004 (×) and this work (◆). Values for the narrow strong 6613 Å DIB are taken from Thorburn et al. 2003 (·), Sonnentrucker et al. 1997 (⋄), Rawlings et al. 2003 (□), Tuairisg et al. 2000 (•) and this work (◆). The data sets plotted in the three panels, constitute a non-exhaustive compilation of lines of sight that probe a range of Galactic interstellar environments. We show in the top panel the two 5780 Å DIB equivalent width versus reddening relations for the interstellar clouds in the line of sight towards HD144217 and HD145797, which are typical for σ and ζ type cloud DIB behaviour, respectively. Errors (not shown in figure) are 5 to 20% in $E_{(B-V)}$ and less than 10% in equivalent width. In all three panels we show the linear regression fit to the plotted dataset (dashed line). We excluded the highly reddened data points from the linear fit: for the 5797 Å DIB the two highly reddened Cygnus targets were excluded; for the 5780 Å DIB 4U 1907+09 was omitted; and for the 6613 Å DIB the Rawlings et al. (2003) data were not included.

in the direction of 4U 1907+09 must be patchy, consisting of a mix of diffuse (e.g. cloud edges) and translucent to dense (e.g. cloud centres) regions. A more detailed view is discussed next.

4.4. Ionisation balance

Diffuse interstellar clouds can be divided in two main types, called σ and ζ, which represent clouds that are edge and core dominated, respectively (Krełowski & Sneden 1993; Cami et al. 1997). Every line of sight towards a bright star samples one or more diffuse interstellar clouds. Whether this line of sight probes predominantly the outer edge of a cloud (σ; where the interstellar radiation field still penetrates significantly) or whether it probes the cloud core (ζ; where the UV field is already significantly attenuated) determines the behaviour of a given DIB carrier. Some DIB carriers are hence more affected by denser cloud regions than others. The difference between σ and ζ type clouds is best observed for the 5780 Å DIB. For the 5797 and 6613 Å DIBs the difference is less clear (see e.g. Fig. 4).

The 5797 and 5780 Å DIB strengths or central depths can be used to infer the local UV irradiation conditions and subsequently, through their ratio, the prevailing ionisation balance (Krełowski et al. 1995; Cami et al. 1997). There are indications that the 5780 Å DIB carrier has a higher ionisation potential than the 5797 Å DIB carrier and thus reaches its maximum strength only in regions with a stronger UV field, whereas the 5797 Å DIB is more easily ionised, and even already largely destroyed when the 5780 Å DIB strength reaches its maximum

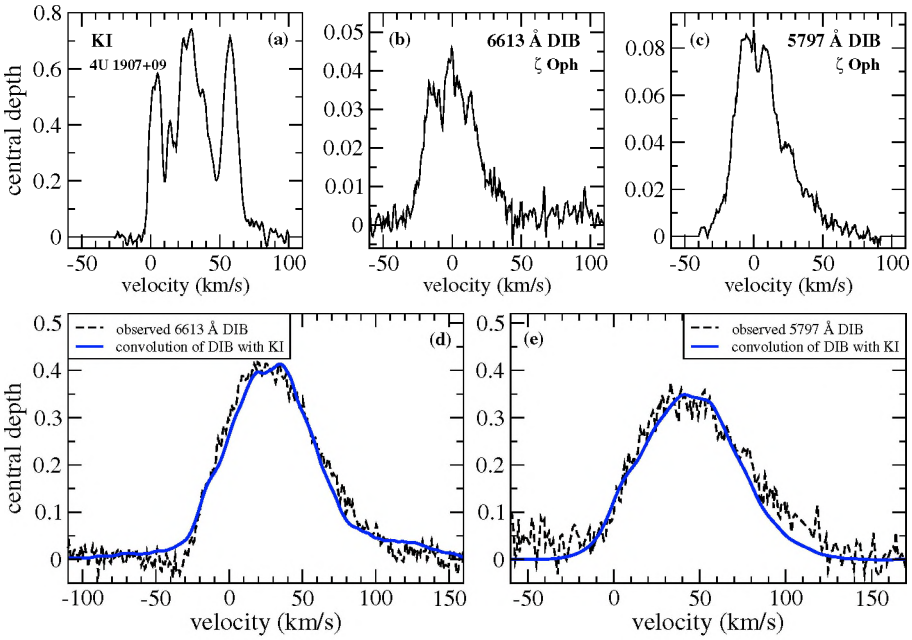

Fig. 5. Panel **a)** shows the K I (7698.98 Å) profile observed towards 4U 1907+09, which gives an indication of the velocity and density distribution of the ISM gas (from Cox et al. 2005). The narrow (intrinsic) 6613 and 5797 Å DIB profiles observed towards HD 149757 (Sarre et al. 1995; Kerr et al. 1998) are shown in panels **b)** and **c)**, respectively. The bottom panels **d)** and **e)** show the result of the convolution (solid) of the narrow single cloud DIBs with the 4U 1907+09 K I profile, respectively, as well as the respective observed 4U 1907+09 DIB profiles (dashed). The convolutions (solid) are scaled in intensity and shifted in velocity to match both the maximum depth and central velocity of the observed profile.

Table 3. Relative strength of 4U 1907+09 DIBs compared to BD +63 1964 and HD 183143 DIBs. The DIBs in 4U 1907+09 are stronger and broader compared to the reference targets. The 9577 and 9632 Å DIBs for BD +63 1964 have been observed tentatively by Vuong (private communication) and are weakened by about a factor of three with respect to HD 183143.

"Family"	DIB	4U 1907+09 / BD +631964	4U 1907+09 / HD 183143	BD +631964 / HD 183143
1	6196	2.61	2.40	0.92
	6613	2.32	2.28	0.98
	5797	2.09	2.88	1.38
	6379	1.65	2.72	1.65
	5849	2.10	4.03	1.92
2	5780	1.67	1.52	0.91
	6284	2.42	1.80	0.75
	6203	1.98	2.20	1.11
C_{60}^+	9577	2.81	0.94	0.33
	9632	3.45	1.15	0.33
ratio $E_{(B-V)}$		3.42	2.70	0.79

(Cami et al. 1997). The 5797/5780 strength ratio is also directly related to the UV extinction properties (Krełowski et al. 1995). Complementary, the central depth ratio for the 5797 and 5780 Å DIBs is related to the column density of CH, CO, and the H_2 fraction. These DIBs are also (anti) correlated to the far UV non-linear rise, thus implying a connection with small dust grains (Megier et al. 2001; Weselak et al. 2004; Megier et al. 2005).

We find an intermediate central depth ratio of 0.75 (Weselak et al. 2004: σ and ζ type clouds have a lower and higher ratio, respectively). Unfortunately, we do not have information on the column densities of the diatomic species CH, CH+ and CN, nor of the H_2 fraction towards 4U 1907+09. Nonetheless, the detected C_2 (2–0) and (1–0) Philips bands (transitions in respectively the 8750–8780 Å and 10 140–10 160 Å spectral range; Fig. 1) clearly indicate cold (dense) components in the diffuse medium (e.g. Van Dishoeck & Black 1989; Gredel 1999; Cecchi-Pestellini & Dalgarno 2002; Scappini et al. 2002). The relative weakness of the 5780 Å DIB and the normal strength of the 5797 Å DIB (Table 4 and Fig. 4) suggest that some dense clumps in the line of sight cause a local attenuation of the UV field (Krełowski & Westerlund 1988; Krełowski et al. 1992), which will then first result in a lower abundance of the 5780 Å DIB. In addition, if the near-IR 9577 and 9632 Å bands are indeed connected to the C_{60} cation, their relative weakness (per unit reddening) would also point to conditions prevailing in translucent/dense clouds, since the weak UV field in these regions would predict a low C_{60} ionisation rate, which would result in a low cation abundance (and a subsequently higher neutral fraction).

The high extinction (A_V = 9.3 mag) shows that this line of sight has an unusually high extinction per kpc ($A_V \approx 2$ mag kpc^{-1}) compared to the general ISM ($A_V \approx 1$ mag kpc^{-1}) again implying denser to translucent clouds. For the total integrated DIB column towards 4U 1907+09 the 5797/5780 DIB strength ratio is 0.49 ± 0.06, which is relatively high. It is close to the ratio r = 0.4 observed for the single ζ-type cloud HD 149 757 (Krełowski & Sneden 1995). The ratio is also similar to that for Cyg OB2-41, r = 0.36, although this line of sight shows a significantly reduced strength of both DIBs with

Table 4. Sightlines towards five reddened HMXBs. The name of the X-ray source, colour excess $E_{(B-V)}$, visual extinction A_V, total to selective visual extinction R_V, H I column density, distance and the 5797, 6613, 5780 Å DIB and K I equivalent widths are tabulated.

HMXB	$E_{(B-V)}$[a]	A_V[b]	R_V[c]	log N(H I)[d]	d	W(DIB)/$E_{(B-V)}$ (Å)[e]			W(K I)[e]
	(mag)	(mag)		(cm^{-2})	(kpc)	5797	6613	5780	(mÅ)
4U 1700-37	0.52	1.7	3.3	21.48	1.8	0.11	0.20	0.63	142 ± 5
Vela X-1	0.7	1.3	1.9	21.37	2.0	0.14	0.20	0.40	166 ± 5
Cen X-3	1.4	4.3	3.1	21.89	5.4	0.13	0.19	0.49	not observed
GX 301-02	1.8	4.8	2.7	21.93	5.3	0.13	0.18	0.48	350 ± 1
4U 1907+09	3.45	9.5	2.75	22.22	5	0.16	0.20	0.33	861 ± 11

[a] $E_{(B-V)}$ for 4U 1907+09 from Cox et al. (2005); for the other sources $E_{(B-V)}$ is taken from Van Paradijs & McClintock (1995); Van Paradijs & White (1995). [b] A_V values derived from extinction maps of Drimmel et al. (2003). These values are consistent with those given by Gorenstein (1975) for 4U 1700-37, Cen X-3 and GX 301-02. For Vela X-1 there is a large discrepancy: Gorenstein (1975) gives A_V = 2.5 mag. [c] from $R_V = A_V / E_{(B-V)}$. [d] N(H I) estimated adopting the relationship of Predehl & Schmitt (1995): $N(\mathrm{H\,I}) = (1.79 \pm 0.03)\, A_V \times 10^{21}$ cm^{-2}. [e] DIB and K I strengths were measured in high-resolution spectra that were obtained by one of us (LK) with 1.52 m/FEROS for 4U 1700-37 and Vela X-1 (30-11-1998), and with VLT/UVES for Cen X-3 (12-01-2000) and GX 301-02 (13-02-2000) (ESO programs: 60.A-9022, 63.H-0456 and 67.C-0281).

respect to the Galactic trend. The weak 5910.7 and 6010.0 Å DIBs, typical for respectively ζ and σ type clouds, are both seen in this line of sight.

4.5. Velocity broadening of DIBs

For further details on the conditions of individual clouds in this line of sight we need to unravel the individual cloud contributions to the total DIB profile. In this section we reconstruct an observed narrow DIB from a single cloud DIB profile and the information on the ISM structure provided by the atomic K I profile.

The increase in FWHM can be explained by Doppler broadening, the effect that individual interstellar clouds in the different spiral arms contribute at different projected velocities to the observed DIB profile. The Doppler splitting in narrow DIB profiles was already established by Herbig & Soderblom (1982) and Westerlund & Krełowski (1988a,b). For the line of sight towards 4U 1907+09 the narrow 6613 and 5797 Å DIB profiles, together with that of K I, offer an opportunity to test this broadening effect for a sightline with a complex extended ISM structure.

Noteworthy is that the 6613 Å DIB carrier has been shown to follow the Ca II distribution (Sonnentrucker et al. 1999), indicating that this DIB carrier has a spatial distribution that more closely follows that of ionised species (e.g. Ca II) that trace the warm intercloud medium rather than that of neutral species (e.g. Na I) that probe the denser cloud cores. Unfortunately, the Ca II lines have not been detected towards 4U 1907+09 due to the poor spectral quality caused by the severe reddening. Krełowski et al. (1998) reported a correlation between K I (and more tentatively also for Ca I) and the narrow DIB carriers at 5797 and 6379 Å (abundant in regions where energetic UV photons are scarce), but not with the broader 6284 and 5780 Å DIBs (resistant to UV photons). For our line of sight the interstellar velocity structure can only be derived from the K I lines. Grain depletion is not expected for potassium as this element is not incorporated in interstellar dust particles. Thus, we have related the neutral species K I to the 6613 and 5797 Å DIBs. We also chose these DIBs because they are both narrow and strong (*FWHM* $\approx$ 0.9 Å or $\approx$40 km s^{-1} for single cloud lines of sight). The "intrinsic" (i.e. high resolution, high signal-to-noise) single cloud velocity profiles of the narrow 6613 and 5797 Å DIBs towards HD 149757 (Sarre et al. 1995; Kerr et al. 1998; see Fig. 5, panel b and c) are convolved with the K I velocity profile (Fig. 5, panel a). The spectra have to be converted from an absorption to a depth (with respect to the continuum) profile (e.g. the convolution recipe requires the signal to be zero on both sides of the profile). The result of this convolution is then shifted and scaled to match the observed central velocity and central depth, respectively. The final profiles are shown in panels d and e of Fig. 5.

The observed DIB broadening (width and shape) and subsequent loss of substructure (Fig. 5) can thus be explained adequately and accurately by Doppler "splitting" due to the observed (velocity) distribution of the interstellar medium. More importantly, this result shows that K I can be used as a rough tracer of the (velocity) distribution of both the 6613 and 5797 Å DIB carriers. However, there are subtle differences between the observed and inferred DIB profiles. For example, the convolution of the 5797 Å DIB slightly underestimates the high-velocity wing of the observed profile. Although difficult to quantify one could argue that the low velocity K I component does not fully reproduce the observed DIB profile. However, it should be noted that such small differences are sensitive to small changes in the adopted high resolution "intrinsic" single cloud DIB profiles, as well as the central depth scaling.

4.6. DIB strength versus column density of the neutral elements H I and K I

DIB strength correlations between many lines of sight have been studied, using bright background sources like OB-type stars and supernovae. Most of these studies focus on the correlation with reddening (see also Sect. 3.1); only a handful have

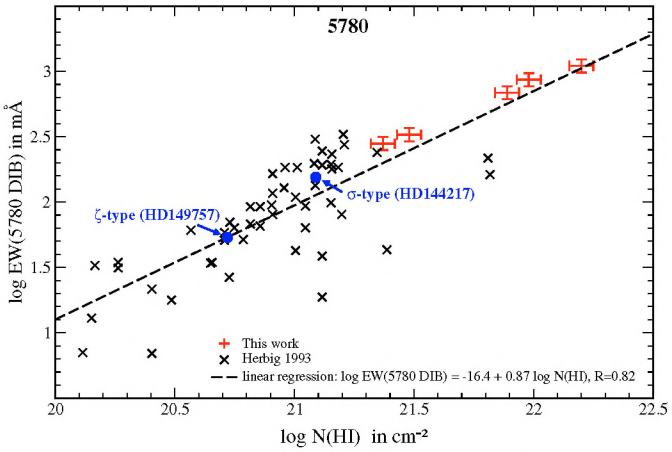

Fig. 6. The 5780 DIB strength versus the H I column density towards the HMXB systems from this work (+) and the lines of sight in Herbig (1993) (×). The correlation coefficient for the HMXB subset is 0.93, while that of the combined data is 0.82.

gone beyond (e.g. Herbig 1993; Krełowski et al. 1999; Weselak et al. 2004; Galazutdinov et al. 2004). Next, we discuss the correlation of the 5780 and 5797 Å DIBs with neutral hydrogen and extend it with four reddened lines of sight to distant targets.

To this aim we examined lines of sight towards four other highly reddened OB stars in high-mass X-ray binary systems. Their OB companions have been identified following the detection of the X-ray sources which do not suffer much from interstellar extinction. As a consequence, these systems constitute a sample with no bias to reddening or distance. Also, these lines of sight have been well studied and thus much additional information is available. In Fig. 6 we plot the 5780 DIB strengths for these five X-ray binary systems, together with the data from Herbig (1993) as a function of the interstellar neutral hydrogen column density. The former are obtained from X-ray observations, and from A_V (see Table 4). The spectra were obtained by one of us (LK) with either VLT/UVES or 1.52 m/FEROS. A summary of the respective observational details is given in Table 4.

For these four targets the H I column density correlates very well with the 5797, 6613 and 5780 DIBs (correlation coefficients of 0.99, 0.95 and 0.93, respectively). Including the 5780 Å DIB data from Herbig (1993) gives a correlation coefficient of 0.82. This indicates that the carrier of the broader 5780 DIB is better correlated to the gas tracer H I than to the dust tracer $E_{(B-V)}$, especially for higher column densities of diffuse ISM (see both Figs. 4 and 6). The correlation with neutral hydrogen could in principle be applied to any line of sight to estimate the interstellar H I column density by observing the strength of the 5780 DIB, or vice versa. Complementary, the 5797/5780 ratio can possibly be used to estimate the molecular hydrogen fraction (Weselak et al. 2004).

For the three targets in Table 4 the DIB and K I equivalent widths are well correlated, and the respective absolute values are in line with the recent correlation study by Galazutdinov et al. (2004). Only GX 301-02 has stronger DIBs than expected from the K I line. Possibly, some saturation of K I may affect the observed equivalent width.

5. Discussion and conclusion

High resolution and high signal-to-noise UVES spectra are used to study a unique line of sight through a large column of dust and gas in the direction of 4U 1907+09. We investigated in detail the interstellar absorption spectrum, which results in the detection of some of the strongest diffuse interstellar bands (DIBs) measured to date. The line of sight towards 4U 1907+09 passes through a complex ensemble of diffuse and translucent clouds. We detect a total of 180 DIBs of which we confirm about 25 previously tentative DIBs. The comparison with BD +63 1964 and HD 183143 clearly shows the wealth and strength of the DIBs observed in this line of sight. The total observed DIB profile is a composite of DIBs formed in all individual interstellar clouds at different intervening distances, e.g. spiral arm structure, up to the binary system at 5 kpc. The Doppler broadening of DIBs is evidence to this effect. The Doppler broadening analysis shows that the neutral potassium can be used to infer the narrow 6613 and 5797 Å DIB carrier distribution. This result indicates that these two DIBs might be more related to the cooler (cloud core) medium, than to the hotter intercloud regions, as argued by Sonnentrucker et al. (1999). Due to poor signal to noise we have no access to other strong (di)atomic lines, like Ca II or CH, in the blue region of the spectrum, which prevents any further trace species analyses.

How the DIB carriers are distributed throughout the Galaxy is not known. The analyses of distant, and thus highly extincted, lines of sight are crucial to infer the conditions and composition of dust and gas throughout the Galactic disk (i.e. towards both the Galactic center and the outer edge). The increase in DIB strength as a function of reddening for this highly reddened line of sight is consistent with previous work (e.g. Herbig 1993). We expand the DIB strength versus reddening relationship to higher values of $E_{(B-V)}$. Whereas the 5780 Å DIB is weaker than expected from the linear correlation with reddening, the 5797 Å DIB is of expected strength with respect to reddening.

In addition we confirm that both the 5797 and the 5780 Å DIB strengths are closely correlated to both the H I and K I column densities (Fig. 6 and Table 4 in Sect. 4.6). This suggests that, for diffuse clouds with very little ionised hydrogen, the total column density of these (i.e. 5797, 5780 and 6613 Å) DIB carriers is more accurately traced by the neutral hydrogen (gas) than by reddening (dust). For the 6613 Å DIB this is in agreement with the observed correlation with K I. Note that Galazutdinov et al. (2004) find in their (more extensive) correlation study that the 6613 Å DIB is not well correlated with the K I, nor with the Ca II equivalent width.

From the 5797/5780 DIB strength ratio we infer that the line of sight towards 4U 1907+09 passes through an ensemble of clouds, ranging from diffuse, translucent to dense clouds. The ratio is in between that of a typical σ and a ζ-type cloud, not unexpected for complex lines of sight (e.g. Rawlings et al. 2003). The gas and dust quantities and properties influence the charge state balance of DIB carrier molecules. Recombination

Table 5. Line of sight comparison. To illustrate how the line of sight towards 4U 1907+09 relates to the other well studied lines of sight in our Galaxy, we summarise dust, gas and DIB properties. DIB strengths for Cyg OB2-41 (VI Cyg 12) from Chlewicki et al. 1986 (except for λ6613 taken from Rawlings et al. 2003 and λ6379 taken from Bromage & Nandy 1973). DIB strengths for HD 144217 and HD 149757 are from Sollerman et al. (2005). For HD 183143, BD +63 1964 and Cyg OB2-41 the $N(H_2)$ is inferred from N(CH) (Jenniskens et al. 1992), and N(H I) from N(H)=5.8 $\times$ 10^{21} $E_{(B-V)}$ and $N(H) = N(H\,I) + 2\,N(H_2)$. N(CH) via EW(CH) (Krełowski et al. 1999) for HD 183143 and BD +63 1964, and from Scappini et al. (2000) for Cyg OB2-41.

	4U 1907+09	HD 183143	BD +63 1964	Cyg OB2-41	HD 144217 (σ)	HD 149757 (ζ)
log N(H I)	22.22	21.69	21.59	22.25	21.09	20.72
log $N(H_2)$		21.10	20.98	21.01	19.83	20.65
$E(B-V)$ (mag)	3.45	1.28	1.01	3.4	0.20	0.32
R_V	2.75	3.3	3.1	~3.1	4.0	3.09
A_V (mag)	9.5	4.2	3.1	~10.5	0.80	0.99
$N(H\,I)/A_V$ ($\times 10^{21}$)	1.75	1.17	1.25	1.69	1.54	0.53
DIB strength (mÅ) per $E(B-V)$ (and per A_V)						
5797	156 (57)	146 (45)	255 (83)	100 (32)	110 (28)	84 (27)
5780	339 (123)	602 (183)	692 (225)	273 (88)	800 (200)	206 (67)
6613	200 (73)	250 (76)	311 (101)	109 (35)	200 (50)	134 (43)
6284	1009 (366)	1507 (459)	1424 (464)	645 (209)	1950 (488)	347 (112)
6379	84 (31)	84 (25)	174 (57)	76 (25)	70 (18)	75 (24)

processes in regions with higher electron density and higher dust concentrations attenuating UV photons subsequently influence the local excitation of DIB carriers resulting in a change in charge state.

Table 5 compiles gas and dust properties, and strengths of strong DIBs, in sightlines that are well studied for their environmental conditions. It can be seen that the 2 sources which probe an extended sightline of several kpc (5 kpc for 4U 1907+09 and 2 kpc for Cyg OB2-41) show a strong similarity in band strength of the strongest DIBs and in DIB ratios. Both highly extincted sources also share similar gas and dust properties as inferred from R_V, $N(H_2)$ and A_V. This trend can be extended to the nearby source HD 149757 (ζ Oph at ~150 pc), which probes a much smaller column density of gas and dust (one tenth). The observed DIB strength ratios are similar, although the column density of DIB carriers per unit reddening is two times less. ζ Oph is known to be located behind a relative dense cloud (core) (Snow & Krełowski 1994). The comparison of ζ Oph data with the two extended and extincted sightlines indicates that the latter are intersected by a large number of ζ type clouds, attenuating a substantial amount of UV photons. This affects in particular the carriers of the 5780 and 6284 Å DIBs which need sufficient UV exposure to be excited. The DIB strength per unit reddening for ζ Oph compared to 4U 1907+09 and Cyg OB2-41 is a factor two weaker. Looking at well studied sightlines with enhanced DIB strength such as BD +63 1964 and HD 144217 indicates a much higher 5780 Å DIB strength per unit reddening. From the H I column densities we infer that there is 30 times more gas in the line of sight towards 4U 1907+09 (which correlates with a factor 30 in distance) and only 10 times as much dust compared to the sightline towards ζ Oph. Correcting for the gas-to-dust ratio in both sources (see Table 5) leads to a DIB strength of both sources that is very similar, within the error bars, for the 5797 and 5780 Å DIBs. This applies also to Cyg OB2-41. For the 4U 1907+09 and HD 144217 (σ type cloud) columns we find that, although the gas-to-dust ratio is similar, the 5797 Å DIB responds differently. This strongly supports the idea that the local UV ionization condition drives the chemistry of DIB carriers.

Studying different (highly) reddened lines of sight (see e.g. Sect. 4) can reveal environmental properties of the diffuse interstellar bands (DIBs) carriers. Only large telescopes and high resolution spectrographs (such as UVES on the VLT) have made it feasible to probe highly extincted regions in the optical domain. This work represents only one of the first steps in optical studies of extincted and distant regions which may shed light on the behaviour of DIBs throughout the Galaxy. In the search for the nature of the DIB carrier, highly reddened lines of sight are complementary to single cloud line of sight studies.

Acknowledgements. The authors thank ESO and the Paranal staff for their support in using the UVES instrument on the VLT. Constructive comments from the referee are highly valued and have resulted in significant improvements of the paper. NLJC acknowledges support from NOVA and PE from NWO-VI (016.023.003). This research has made use of the SIMBAD database, operated at CDS, Strasbourg, France, and of the NASA Astrophysics Data System.

References

Benvenuti, P., & Porceddu, I. 1989, A&A, 223, 329
Bromage, G. E., & Nandy, K. 1973, A&A, 26, 17
Cami, J., Sonnentrucker, P., Ehrenfreund, P., & Foing, B. H. 1997, A&A, 326, 822
Cecchi-Pestellini, C., & Dalgarno, A. 2002, MNRAS, 331, L31
Chlewicki, G., Van der Zwet, G. P., Van Ijzendoorn, L. J., Greenberg, J. M., & Alvarez, P. P. 1986, ApJ, 305, 455
Cox, N. L. J., Kaper, L., & Mokiem, M. R. 2005, A&A, 436, 661
Drimmel, R., Cabrera-Lavers, A., & López-Corredoira, M. 2003, A&A, 409, 205

Ehrenfreund, P., Cami, J., Dartois, E., & Foing, B. H. 1997, A&A, 318, L28
Ehrenfreund, P., & Foing, B. H. 1996, A&A, 307, L25
Foing, B. H., & Ehrenfreund, P. 1994, Nature, 369, 296
Foing, B. H., & Ehrenfreund, P. 1997, A&A, 317, L59
Galazutdinov, G. A., Musaev, F. A., Krełowski, J., & Walker, G. A. H. 2000, PASP, 112, 648
Galazutdinov, G. A., Manicò, G., Pirronello, V., & Krełowski, J. 2004, MNRAS, 355, 169
Giacconi, R., Kellogg, E., Gorenstein, P., Gursky, H., & Tananbaum, H. 1971, ApJ, 165, L27
Gorenstein, P. 1975, ApJ, 198, 95
Gredel, R. 1999, A&A, 351, 657
Herbig, G. H. 1993, ApJ, 407, 142
Herbig, G. H. 1995, ARA&A, 33, 19
Herbig, G. H., & Soderblom, D. R. 1982, ApJ, 252, 610
Jenkins, E. B. 1996, ApJ, 471, 292
Jenniskens, P., & Desert, F.-X. 1994, A&AS, 106, 39
Jenniskens, P., Ehrenfreund, P., & Desert, F.-X. 1992, A&A, 265, L1
Josafatsson, K., & Snow, T. P. 1987, ApJ, 319, 436
Kaufer, A., D'Odorico, S., & Kaper, L. 2000, UVES User Manual
Kerr, T. H., Hibbins, R. E., Fossey, S. J., Miles, J. R., & Sarre, P. J. 1998, ApJ, 495, 941
Krełowski, J., & Walker, G. A. H. 1987, ApJ, 312, 860
Krełowski, J., & Westerlund, B. E. 1988, A&A, 190, 339
Krełowski, J., & Sneden, C. 1993, PASP, 105, 1141
Krełowski, J., & Sneden, C. 1995, Diffuse Interstellar Bands in Individual Sightlines (ASSL Vol. 202: The Diffuse Interstellar Bands), 13
Krełowski, J., Snow, T. P., Seab, C. G., & Papaj, J. 1992, MNRAS, 258, 693
Krełowski, J., Sneden, C., & Hiltgen, D. 1995, Planet. Space Sci., 43, 1195
Krełowski, J., Galazutdinov, G. A., & Musaev, F. A. 1998, ApJ, 493, 217
Krełowski, J., Ehrenfreund, P., Foing, B. H., et al. 1999, A&A, 347, 235
Lanz, T., & Hubeny, I. 2003, ApJS, 146, 417
Megier, A., Aiello, S., Barsella, B., Casu, S., & Krełowski, J. 2001, MNRAS, 326, 1095
Megier, A., Krełowski, J., & Weselak, T. 2005, MNRAS, 196
Moutou, C., Krełowski, J., D'Hendecourt, L., & Jamroszczak, J. 1999, A&A, 351, 680
Porceddu, I., Benvenuti, P., & Krełowski, J. 1991, A&A, 248, 188
Predehl, P., & Schmitt, J. H. M. M. 1995, A&A, 293, 889
Rawlings, M. G., Adamson, A. J., & Whittet, D. C. B. 2003, MNRAS, 341, 1121
Russeil, D. 2003, A&A, 397, 133
Sarre, P. J., Miles, J. R., Kerr, T. H., et al. 1995, MNRAS, 277, L41
Scappini, F., Casu, S., Cecchi-Pestellini, C., & Olberg, M. 2002, MNRAS, 337, 495
Scappini, F., Cecchi-Pestellini, C., Codella, C., & Dalgarno, A. 2000, MNRAS, 317, L6
Schmidt-Kaler, T. 1982, Bulletin d'Information du Centre de Données Stellaires, 23, 2
Schwartz, D. A., Griffiths, R. E., Bowyer, S., Thorstensen, J. R., & Charles, P. A. 1980, AJ, 85, 549
Snow, T. P., & Krełowski, J. 1994, in ASP Conf. Ser., 64
Sollerman, J., Cox, N., Mattila, S., et al. 2005, A&A, 429, 559
Sonnentrucker, P., Cami, J., Ehrenfreund, P., & Foing, B. H. 1997, A&A, 327, 1215
Sonnentrucker, P., Foing, B. H., & Ehrenfreund, P. 1999, Adv. Space Res., 24, 449
Thorburn, J. A., Hobbs, L. M., McCall, B. J., et al. 2003, ApJ, 584, 339
Tuairisg, S. Ó., Cami, J., Foing, B. H., Sonnentrucker, P., & Ehrenfreund, P. 2000, A&AS, 142, 225
Van Dishoeck, E. F., & Black, J. H. 1989, ApJ, 340, 273
Van Kerkwijk, M. H., Van Oijen, J. G. J., & Van den Heuvel, E. P. J. 1989, A&A, 209, 173
Van Paradijs, J., & McClintock, J. E. 1995, Optical and Ultraviolet Observations of X-ray Binaries, ed. W. H. G. Lewin, J. Van Paradijs, & E. P. J. Van den Heuvel (Cambridge: Cambridge Univ. Press), 58
Van Paradijs, J., & White, N. 1995, ApJ, 447, L33
Weselak, T., Galazutdinov, G. A., Musaev, F. A., & Krełowski, J. 2004, A&A, 414, 949
Westerlund, B. E., & Krełowski, J. 1988a, A&A, 203, 134
Westerlund, B. E., & Krełowski, J. 1988b, A&A, 189, 221
Wszołek, B., & Godłowski, W. 2003, MNRAS, 338, 990

Online Material

Table 2. Observed wavelength (λ in Å) (in heliocentric rest frame), full width at half maximum (F in Å), equivalent width (W in mÅ) and the statistical error on equivalent width (σ in mÅ) of the DIBs detected towards 4U 1907+09 are given in Cols. 1 to 4, respectively. Corresponding values for the comparison targets BD +63 1964 (λ < 6650 Å; Tuairisg et al. 2000) and HD 183143 (λ > 6650 Å; Jenniskens & Desert 1994, JD94) are given in Cols. 5 to 8. 4U 1907+09 features that are only tentative are put into parenthesises. For spectral regions not covered by our observations we use "x". Parameters for all DIBs (both for 4U 1907+09 and reference targets) are determined by fitting Gaussians. For 4U 1907+09 it is not always possible, due to broadening and/or limited signal-to-noise, to decompose the DIB spectrum in a similar way as has been done for the reference spectra. Where possible we indicate with curly brackets how different DIB complexes are related to each other. A large number of the very weak DIBs ($\leq$ 10 mÅ) are not detected, especially those in regions contaminated with telluric lines, or regions affected by small scale fringing (above 7000 Å). Column 10 (N) lists a "+" for the positive identification of a hitherto tentative DIB. A non-detection of a tentative DIB is indicated with "–". And a "G" refers to a new DIB from the Galazutdinov et al. (2000) survey. A "?" points out a unidentified feature. The expected stellar contamination is very small, and mostly negligible in deriving the EW. We indicate also in Col. 10 the possible stellar line contamination as predicted by the Lanz & Hubeny (2003) O-star model atmosphere with T = 30,000 K and log g = 3.00 (see also the main text).

4U 1907+09				BD +63 1964				
λ	F	W	σ	λ	F	W	σ	N
4727.5	5.9	800	50	4726.35	1.70	117	7	
				4728.35	1.54	50	4	
				4762.57	2.89	143	5	
		6250	100	4764.66	29.0	546	55	
				4780.10	1.74	55	4	
4826.5	17.1	1010	100	4825.94	20.4	347	27	
				4880.4	1.35	22		JD94
4883.3	29.0	1900	150	4882.56	14.9	466	20	
				4951.05	0.67	8	2	–
				4963.03	21.3	218	12	
4964.4	0.9	120	15	4963.89	0.71	31	3	
				4968.87	6.54	65		
				4979.28	1.29	14		
				4984.78	0.67	19	2	
				5038.59	26.9	344	33	
				5061.56	0.64	9	2	–
				5098.84	0.48	5		
5112.6	6	410	30	5110.81	2.45	30	6	
				5170.81	0.87	18	3	–
5176.7	1.5	61	8	5176.00	0.76	9	2	+
				5176.67	3.50	34		
5236.7	2.3	130	10	5236.34	1.95	49	3	+
				5247.91	0.39	6	3	–
5351.1	2.7	62	9	5349.16	1.16	10	3	–
5359.5	4.5	126	10	5359.58	3.92	41	9	
5364.3	3.3	210	11	5363.78	2.54	76	7	
5369.5	4.6	99	10	5370.36	3.25	29	4	+
5405.2	1.9	130	8	5404.52	1.06	33	2	
5422.0	15.7	520	18	5418.39	8.85	109	9	
5419.3	1.1	53	9	5419.05	1.07	20	2	+
				5428.63	1.11	12		
5450.7	12.9	919	27	5449.76	9.53	290	12	
				5450.95	31.2	696	22	
5488.2	4.6	401	14	5487.54	2.51	82	8	
				5487.90	6.67	166	12	
				5490.52	0.75	8	2	+
5494.8	1.1	76	8	5494.10	0.86	51	3	
5498.0	2.5	29	8	5497.00	2.17	22	5	+
5503.5	0.2	8	3	5503.16	0.42	5	2	–
5506.6	0.7	7	3	5506.06	0.58	7	2	+
5508.6	4.7	365	12	5508.03	2.77	103	6	
				5508.2		26		O III
5513.1	0.9	47	7	5512.66	0.69	19	2	+
5516.8	1.5	24	6	5515.97	1.06	8	3	+
				5524.47	0.91	11	2	

Table 2. (continued)

4U 1907+09				BD +63 1964				
λ	F	W	σ	λ	F	W	σ	N
5536.2	3.3	270	11	5535.26	1.35	28	4	
				5537.51	5.42	95	18	
				5539.73	1.48	14		
5542.3	1.4	41	6	5541.78	0.68	13	3	
5545.5	0.9	48	6	5545.02	0.85	38	4	
5546.5	1.7	77	6	5546.52	0.68	11	3	+
								?
5557.1	1.0	25	4	5556.27	0.90	9	3	+
				5563.06	0.85	7	3	–
				5569.08	0.35	6	2	–
x				5594.54	0.86	16	3	
x				5597.38	2.59	16	4	
x				5600.49	1.17	9	2	
x				5609.96	2.14	33	6	
x				5645.43	0.71	11	2	
5706.0	3.3	313	13	5705.10	2.75	166	10	
5712.0	2.6	113	10	5709.40	1.71	49	9	
5720.2	1.2	48	10	5719.68	1.04	31	4	
5748.1	3.8	135	13	5746.21	2.84	52	4	
				5760.64	0.61	5	3	
5762.5	2.7	101		5762.80	0.95	16	3	
5767.4	2.9	218		5766.17	1.08	41	3	
5769.9	1.3	69		5769.32	1.26	15	2	
5773.5	2.9	219		5772.67	1.45	32	3	
5784.2	16.2	1450		5776.13	15.2	420	31	
5777.1	2.2	140	10	5776.21	2.00	28	4	
5781.2	2.6	1170		5780.55	2.22	699	4	
(5785.4)				5784.86	0.92	9	2	
(5789.9)				5789.04	1.16	15	3	
5793.9	0.6	22	5	5793.13	0.95	11	2	
5795.7	0.9	50	4	5796.07	6.65	155	16	
5797.8	1.4	539	8	5797.08	0.96	258	15	
				5806.52	1.54	15		
				5810.21	1.74	25	7	
				5815.80	0.65	4	2	
				5818.47	0.81	8	3	
				5819.6				G
				5821.2				G
5828.9	3.6	47	6	5828.56	0.87	15	2	
5838.7	0.8	14		5837.92	0.52	6	2	
				5840.62	0.64	9	3	
				5842.38	0.45	6	2	
5844.5	4.7	255	38	5843.30	0.36	5	3	
				5843.69	0.31	4	3	
				5844.28	4.61	87	11	
				5844.95	0.65	10	3	
5850.3	1.5	250	29	5849.81	1.07	119	2	
				5854.85	2.13	17	5	
				5855.6				G
				5897.7				G
5901.4	0.3	16	3	5900.58	0.75	12	3	
5911.2	0.6	26	4	5910.54	0.89	23	3	
				5922.2				G
5924.4	1.5	102	5	5923.51	0.89	34	3	
5926.7	1.4	64	4	5925.82	0.90	20	3	
5945.9	0.7	27	5	5945.53	0.72	10	2	

Table 2. (continued)

4U 1907+09				BD +63 1964				
λ	F	W	σ	λ	F	W	σ	N
5947.6	1.7	84	5	5947.29	0.95	35	3	
5949.6	1.2	50	5	5948.87	0.71	10	3	
5959.6	1.4	66	4	5958.89	1.28	32	3	+
				5963.7				G
				5966.7				G
5971.9	11.3	510		5970.3				G
				5973.78	0.74	10	2	–
				5975.66	0.49	9	2	
				5976.7		25		Fe III
5983.5	2.5	96	7	5982.77	1.23	17	3	
				5986.60	1.30	13	3	
5989.0	1.9	55	6	5988.04	0.91	12	3	
				5989.51	0.95	7	2	
5996.4	1.0	32	5	5995.73	0.84	9	4	
				6004.6		31		Fe III
6005.8	2.6	123	9	6004.80	2.92	36	3	
6011.3	4.2	368	7	6010.48	2.90	88	4	
6020.5	1.9	75	8	6019.45	0.58	9	2	
6028.3	2.6	103	9	6027.09	2.28	37	4	
				6030.5				G
				6036.8		36		He II
6038.0	1.7	81	8	6037.47	2.26	39	3	
6044.2	14.0	680	100	6042.84	14.3	296	32	
6060.9	2.2	55	6	6059.88	1.20	15	5	
				6061.52	0.86	8	4	–
6065.9	2.1	65	6	6065.19	0.90	15	5	
6068.8	0.9	35	1	6068.45	1.34	8	4	+
6071.8	0.7	22	4	6071.08	2.29	16	5	
				6084.94	1.13	9	2	–
6090.3	0.7	61	4	6089.79	0.68	43	2	
				6096.3				G
				6102.48	1.77	12		
6108.6	1.8	47	4	6108.14	0.60	10	2	
6113.9	1.3	84	5	6113.20	1.02	44	3	
6117.4	1.3	61	6	6116.74	0.86	13	2	
				6118		67		He II
6119.0	0.3	11	3	6118.66	0.43	5	2	+
6140.4	1.3	61	5	6139.94	0.64	18	12	
				6141.9				G
6146.1	0.3	10	3	6145.41	0.96	9	9	–
6148.5	1.8	30	10	6147.02	0.90	5	2	+
6152.2	2.3	20	10	6151.15	1.44	15	2	+
(6159.1)				6158.5				G
6162.5	0.7	18	6	6161.83	0.91	11	2	+
6166.3	1.5	54	7	6165.72	1.56	15	3	+
				6170			72	He II
				6170.71	1.31	15	3	–
6175.4	21.8	1985	20	6173.65	23.1	907	22	
				6177.72	1.91	14	3	–
6187.6	2.7	81	6	6185.89	0.93	15	3	–
				6187.19	1.24	19	3	+
6190.3	0.7	16	4	6189.31	1.27	14	3	
6195.2	0.6	15	3	6194.57	0.31	5	2	
				6194.98	0.28	5	2	
6196.8	1.3	206	3	6195.99	0.68	79	3	
6199.6	1.2	23	3	6198.82	0.68	6	3	

Table 2. (continued)

4U 1907+09				BD +63 1964				
λ	F	W	σ	λ	F	W	σ	N
6203.8	1.6	275	6	6203.06	1.30	139	13	
6205.1	5.9	589	6	6204.22	4.92	135	9	
				6207.52	9.34	132	17	
6213.0	2.6	136	5	6211.74	1.27	22	2	
				6212.7	1.23	12		
				6212.95	0.52	4	2	
6216.1	1.6	55	4	6215.80	1.84	20	3	
6221.6		24	3	6220.86	0.84	11	3	
6224.1		22	3	6223.53	0.59	6	2	
6226.7		26	3	6226.02	0.82	11	2	
6234.7	1.2	48	4	6234.01	0.80	28	4	
				6236.71	1.07	10	4	
6245.1	1.9	83	4	6244.42	0.92	13	4	–
				6245.36	2.22	28	3	
6251.4	1.1	24	3	6250.77	1.40	16	3	+
6270.5	2.6	538	7	6269.82	1.22	84	5	
				6270.45	4.34	86	11	
				6278.17	1.16	10	5	
				6280.48	1.03	15	5	
6283.89	11.73	2650	500	6283.30	10.1	899	45	
6285.08	3.0	830	20	6284.09	2.71	540	11	
				6287.57	0.52	13	4	
				6289.70	1.58	21	6	
6302.9	1.94	81	20	6302.29	3.19	31	3	+
6309.3	4.96	290	10	6308.92	2.08	47	3	
				6311		107		He II
				6311.53	23.0	268	32	
				6316.0				G
				6317.1				G
6318.9	4.3	301	8	6317.75	2.97	75	11	
				6318.3				G
6325.5	1.4	53	4	6324.81	1.20	22	6	
6330.8	2.6	79	6	6330.14	0.98	16	2	
6340.3	0.7	13	3					?
6347.1	6.3	151	9					?
6354.3	2.6	116	6	6353.18	2.09	46	3	
6359.3	1.2	20	5	6358.54	1.88	20	3	+
6362.3	33.7	1189	21	6360.21	30.0	834	55	
6363.5	2.5	99	6	6362.23	1.66	31	4	
6367.8	1.0	41	5	6367.28	0.67	18	2	
6369.9	2.6	112	5	6368.6				G
				6371.92	0.74	6	3	
6377.1	1.9	217	5	6376.02	0.64	27	4	
				6376.57	1.80	52	7	
6379.8	1.1	291	5	6379.22	0.81	176	3	
6397.7	1.7	109	5	6396.95	1.35	39	3	
6400.7	2.0	77	5	6400.37	1.10	18	2	
6410.7	0.2	4	2	6410.08	0.45	6	2	+
6414.7	0.9	23	3	6414.15	0.90	5	3	
6412.5	8.1	316	9	6414.76	8.20	89	9	?
				6417.27	0.61	5	2	
				6418.54	0.71	5	2	
6426.4	1.2	67	4	6425.61	0.93	26	3	
6440.1	1.3	59	4	6439.42	1.25	35	3	
6446.1	1.3	99	4	6445.25	0.83	39	4	
6450.1	1.8	80	5	6449.30	1.16	32	3	

Table 2. (continued)

4U 1907+09				BD +63 1964				
λ	F	W	σ	λ	F	W	σ	N
				6451.6	25.4	403		JD94
6457.0	1.5	92	5	6456.08	1.29	47	3	+
6460.9	0.2	3	2	6460.31	0.73	13	3	
6464.4	1.1	50	4	6463.63	1.06	30	2	+
				6465.5				G
6467.6	1.0	37	3	6466.95	0.79	15	2	+
6469.4	1.2	37	4	6468.7				G
				6474.3				G
				6476.9				G
6483.9	1.3	38	5	6480.48	0.54	8	2	+?
				6489.29	0.64	12	3	–
6494.6	8.3	715	11	6492.17	0.78	11	2	
				6492.92	9.67	155	21	
				6497.79	0.73	6	3	
6521.5	1.9	105	5	6520.95	1.35	35	3	
				6532.1	17.2	664		JD94
6537.2	1.4	29	5	6536.86	0.69	6	3	??
								–
6543.9	0.4	13	4	6543.2				G
				6546.6				G
(6549.9)				6549.1				G
6554.3	1.5	66	4	6553.76	0.79	23	2	+
x				6567.6				G
x				6570.5				G
x				6572.8				G
6592.3	7.3	319	8	6591.03	4.19	101	17	
				6594.1				G
6598.0	1.0	18	4	6597.47	0.79	13	3	
6614.5	1.6	730	12	6613.63	1.14	314	4	
6623.6	1.0	26	4	6622.59	2.07	20	4	
				6630.8				G
				6631.7				G
6633.7	0.8	15	3	6632.86	0.95	13	3	
				6635.50	0.63	7	2	
				6639.34	1.11	11		
x				6644.33	1.43	15	3	–
x				6645.95	0.58	8	2	
x				6654.6				G
x				6660.62	0.82	57	3	
x				6662.25	0.43	5	2	–
x				6665.2				G
x				6672.2				G
x				6681.07	2.01	27	4	
x				6684.83	1.09	8	3	–
x				6686.46	0.63	5	2	–
x				6689.38	0.61	10	3	
x				6691.7				G
x				6694.40	1.19	11	2	
6700.0	1.1	68	5	6699.28	0.99	41	3	
6702.5	1.1	29	4	6701.87	0.83	15	3	
				6707.73	1.38	13	3	–
6710.1	1.1	40	4	6709.65	1.76	16	4	
				6719.58	3.05	20	3	–
				6729.20	0.81	17	2	–
6734.9	2.2	44	6	6733.35	1.28	16	2	?
				6737.1				G
				6741.0	0.97	13		JD94

Table 2. (continued)

4U 1907+09				BD +63 1964				
λ	F	W	σ	λ	F	W	σ	N
x				6765.39	0.86	11	3	–
x				6770.23	0.58	9	2	
x				6789.64	2.54	15	3	
x				6792.54	0.66	11	3	
x				6795.18	0.92	11	4	
x				6801.39	0.95	7	3	
x				6804.82	1.86	13	3	
x				6807.3				G
x				6811.30	0.95	14	3	
x				6812.39	1.03	12	3	

4U 1907+09				HD 183143			
λ	F	W	σ	λ	F	W	N
6844.2	1.5	85	6	6843.44	1.18	35	
				6847.8			G
				6849.6			G
6853.8		<60		6852.90	1.38	24	
				6855.4			G
6861.1		<200		6860.02	0.93	34	
				6864.7			G
6888.7	4.6	340		6886.92	0.73	49	
6920.1	1.1	110	5	6919.25	0.96	50	
6936.2	7	170	11	6939.00	21.3	353	
6945.7	1.6	75	5	6944.53	0.84	33	
6947.5	0.15	7	2	6950.6			G
				6953.6			G
				6963.5			G
6972.5	1.6	43	4	6971.5			G
6974.5	1.1	41	4	6973.6			G
6979.2	1.1	34	4	6978.54	0.81	13	
6983.5	0.9	36	3	6982.5			G
6993.9	1.3	290	4	6993.18	0.96	169	
				6998.4		36	OIII
6999.4	1.3	47	3	6998.7	0.56	9	
(7003.4)				7002.2			G
7021.4	1.9	32	5				?
				7030.4			G
7031.7	1.9	73	5	7031.6			G
				7032.9			G
7046.9	0.9	26	3	7045	0.84	15	
				7048		13	CIII
7054.1	2.8	51	5				?
(7060.5)				7060.0			G
7062.0	1.5	120		7060.8	0.67	29	
7063.7	0.7	67		7062.7	0.60	29	
				7069.6	0.92	41	
7073.7	1.7	32	4	7072.7			G
7075.2	0.4	13	4				?
7078.7	1.3	50	3	7078.0	0.71	18	
7080.8	1.6	36	3				?
7086.2	2.8	82	5	7085.1	2.00	43	
7097.5	0.9	18	3				?
				7099.5	0.40	6	
				7101.1	0.84	10	
				7105.9	2.48	34	
7117.0	0.7	15	3				?
7120.8	1.4	68	4	7119.94	1.44	44	

Table 2. (continued)

4U 1907+09				HD 183143			
λ	F	W	σ	λ	F	W	N
7137.2	1.4	29	4	7136.1	0.82	13	
7139.4	3.0	93	5	7138.0	3.50	60	
7154.9	1.3	29	4	7153.8	0.67	9	
7160.7	1.7	76	4	7159.5			G
7163.8	1.5	66	4	7161.2	2.22	48	
7166.0	0.35	10	2	7163.0			G
7173.6	1.7	55	3				?
7176.0	0.9	42	3				?
7177.3	0.8	44	3				?
7181.4	0.41	18	2	7180.0	0.88	42	
7184.4	0.3	28	3				?
7199.4	2.2	58	4				?
7201.9	1.6	110	4				?
7204.4	1.0	64	4				?
				7223.1	5.36	78	
7225.0	1.7	652	16	7224.2	1.07	333	
7230.0	0.5			7228.3	0.89	27	
				7236.4			G
7250.2	1.0	35	4	7249.3			G
7258.0	1.2	33	4	7257.4			G
7265.5	0.8	56	4	7265.0	1.67	25	
				7268.0			G
7272.9	0.5	36	3				?
7275.4	2.1	117		7274.5	5.06	78	
7277.4	0.8	69	4	7276.7	1.14	38	
				7287.6	0.98	x	
7303.3	2.5	56	6	7302.7	1.99	x	?
7309.8	1.1	34	5				?
7312.7	0.6	15	3				?
7315.3	0.5	15	3				?
7322.9	0.3	18	3	7321.1	1.27	15	
7331.2	3.1	55	4	7330.2	1.42	19	
7335.6	1.7	138	4	7334.33	1.24	64	
7348.3	1.6	35	2				?
7350.8	1.3	52	2	7349.8	0.84	13	
7355.8	1.0	26	2	7354.9	0.64	11	
				7357.2	28.2	215	
7358.7	1.3	113	3	7357.60	1.37	43	
7361.8	1.2	35	3	7360.49	1	21	
7367.7	1.5	139	4	7366.61	1.32	62	
7370.6	1.3	35	3	7369.29	1.04	19	
7377.1	1.9	59	3	7375.9	0.79	12	
7386.8	0.9	29	3	7385.9	0.54	13	
				7398.6	1.08	12	
				7401.7	0.98	14	
7406.5	0.7	24	3	7405.8	0.37	5	
7407.8	1.1	21	3	7406.35	1.22	20	
(7420.0)				7419.1			G
7433.5	17.4	420		7432.07	22.33	654	
(7459.0)				7458.2			G
7470.9	2.0	41	5	7468.9			G
7472.5	0.4	20	5	7470.4			G
7473.3	0.3	16	5	7472.7			G
				7483.0			G
				7484.1			G
7495.6	1.9	53	5	7494.9			G

Table 2. (continued)

4U 1907+09				HD 183143			
λ	F	W	σ	λ	F	W	N
7511.9	3.0	29	8				?
7533.5	1.7	27	6				?
7537.2	2.0	47	6				?
				7558.5	1.50	34	
7560.0	2.5	91	6	7559.3	1.15	20	
7563.2	1.9	212	6	7562.24	1.78	96	
				7569.7	5.5	14	
				7571.7			G
7580.7	0.4	21	4	7579.2	1.15	20	
7582.0	2.3	115	6	7581.2	1.45	44	
7587.0	1.6	33	5	7585.6	0.83	11	
	?			7651.4	2.72	108	
7688.1	3.6	140		7686.5	3.17	96	
				7695.9	0.67	14	
				7705.9	3.53	80	
				7708.0			G
				7709.7	33.5	54	
				7713.5	1.29	17	
				7721.0	1.81	82	
7723.0	1.5	96	7	7721.9	0.79	22	
7728.4	0.35	37	5				C_2
				7748.2	4.53	79	
				7782.3	3.64	68	
7828.1	1.0	56					
7833.7	0.8	79		7832.7	0.84	33	
				7843.9	4.8	74	
				7862.3	0.67	12	
				7904.9	1.04	15	
				7908.8			G
				7915.1	1.85	38	
				7920.7			G
7928.0	16.5	898	21	7927.8	15	504	?
				7935.3	0.95	14	
				7987.9	2.9	69	
8027.3	0.93	100		8026.2	0.79	52	
				8037.2	1.72	45	
				8038.5	3.2	112	
				8125.8			G
				8283.5	1.21	52	
8379.3	0.4	96	14				?
				8439.4			G
x				8530.8	1.73	56	
x				8621.1	1.86	133	
x				8621.2	5.59	312	
x				8648.3	4.17	233	
8764.4	1.1	27	4	8763.5	1.35	13	C_2
8879.2	0.2	17	2				?
9278.7	0.4	25	3				?
9413.8	1.9	106	5				?
9474.9	1.9	118	5				?
9579.0	3.5	250	20	9577.0	4.1	261	
9634.1	3.3	300	20	9632.0	4.0	266	
9881.8	1.9	84	6				?